Journal of Physics B: Atomic, Molecular and Optical Physics

Relativistic many-body calculations of transition probabilities for the $2l_1 2l_2[LSJ]$-$2l_3 3l_4[L'S'J']$ lines in Be-like ions

To cite this article: U I Safronova *et al* 1999 *J. Phys. B: At. Mol. Opt. Phys.* **32** 3527

J. Phys. B: At. Mol. Opt. Phys. **32** (1999) 3527–3545. Printed in the UK PII: S0953-4075(99)01624-7

Relativistic many-body calculations of transition probabilities for the $2l_1 2l_2[LSJ]$–$2l_3 3l_4[L'S'J']$ lines in Be-like ions

U I Safronova, A Derevianko, M S Safronova and W R Johnson
Department of Physics, University of Notre Dame, Notre Dame, IN 46556, USA

Received 5 February 1999, in final form 10 May 1999

Abstract. Reduced matrix elements, oscillator strengths, and transition rates are calculated for $2l_1 2l_2[LSJ]$–$2l_3 3l_4[L'S'J']$ electric-dipole transitions in beryllium-like ions with nuclear charges Z from 6 to 100. Many-body perturbation theory (MBPT), including the Breit interaction, is used to evaluate retarded dipole matrix elements in length and velocity forms. The calculations start with a $1s^2$ Dirac–Fock potential and include all possible $n = 2$ and $n = 3$ configurations. We use first-order perturbation theory to obtain intermediate coupling coefficients and second-order MBPT to determine matrix elements. The transition energies used to evaluate transition probabilities are also obtained from second-order MBPT. The importance of negative-energy contributions to the transition amplitudes in maintaining gauge independence is discussed. Our results for $2s3p\,^{1,3}P_1$–$2s^2\,^1S_0$ transitions are compared with available theoretical and experimental data throughout the isoelectronic sequence. Rates for $2l3l'$ $[J = 1]$–$2s^2\,^1S_0$, $2l3l'$ $[J = 1]$–$2p^2\,^1S_2$, $2l3l'$ $[J = 1]$–$2s2p\,^1P_1$, and $2l3l'$ $[J = 2]$–$2s2p\,^1P_1$ transitions are given graphically for all Z.

1. Introduction

In this paper, second-order relativistic many-body perturbation theory (MBPT) is used to calculate reduced matrix elements, oscillator strengths, and rates for electric-dipole transitions between $n = 3$ and $n = 2$ states in beryllium-like ions with nuclear charges $Z = 6$–100. These calculations follow the pattern of relativistic MBPT calculations of 2–2 transitions in beryllium-like ions given in [1]. Numerous theoretical and experimental studies of rates of 3–2 transitions along the beryllium isoelectronic sequence have been performed during the past 30 years. On the theoretical side, Z-expansion [2–4], model potential [5–8], configuration interaction (CI) [9–13], multiconfiguration Hartee–Fock (MCHF) [14–17], R-matrix [18–20], and multiconfiguration Dirac–Fock (MCDF) [21–23] methods have been used to calculate transition matrix elements.

Compared with the alternatives listed above, calculations based on relativistic MBPT stand out since they are gauge independent order-by-order, provided they start from a local potential, include 'derivative terms' in the second- and higher-orders, and include contributions from negative energies in sums over intermediate states. The present MBPT calculations start from a non-local $1s^2$ Dirac–Fock potential and consequently give gauge-dependent transition matrix elements in lowest order. However, the second-order correlation corrections compensate almost exactly for the gauge dependence of the first-order matrix elements and lead to corrected matrix elements that differ by less than 1% in length and velocity forms throughout the Be isoelectronic sequence. It should be noted that this close agreement is obtained only after contributions from negative-energy states ($\varepsilon < -mc^2$) are included in the second-order matrix elements. Other theoretical approaches that account for electron–electron correlation, such as

the R-matrix method, the MCHF method, or the MCDF method, give transition matrix elements that can (and do) differ substantially in length and velocity forms. In this regard, it should mentioned that even complete relativistic configuration-interaction (CI) calculations, such as those used in [24] to study 2–2 transitions in helium-like ions, lead to differences between length- and velocity-form amplitudes unless negative-energy contributions are included.

Another important feature of MBPT calculations is that all transitions within a given complex of states are treated simultaneously. In this calculation, the model space of unperturbed $2l_1\,2l_2$ states consists of four odd-parity and six even-parity states; the corresponding $2l_3\,3l_4$ space consists of 20 odd-parity and 16 even-parity states. First- and second-order electric-dipole matrix elements are calculated between these unperturbed states leading to 116 distinct uncoupled matrix elements. The uncoupled matrix elements differ in length and velocity form. These uncoupled matrix elements are transformed to give the corresponding 116 transition matrix elements between coupled 'physical' states using first-order intermediate coupling coefficients. The resulting *gauge-independent* coupled dipole matrix elements are combined with second-order energies from [25] to determine oscillator strengths and transition rates.

The present relativistic MBPT calculations are based on the Coulomb + Breit *no-pair* Hamiltonian [26]. The static form of the Breit interaction is used here. It was shown that second-order energies for 3–2 transitions evaluated using this Hamiltonian are in excellent agreement with experiment throughout the Be isoelectronic sequence, and that the relative accuracy of the MBPT calculations increases with increasing Z [25]. Since we consider transitions in high-Z ions here, we include retardation fully in the electric-dipole operator. In each successive order of MBPT, contributions to electric-dipole matrix elements decrease in size by a factor of approximately Z. It follows that MBPT calculations are most suitable for high-Z ions. In the present second-order calculation, one expects errors from omitted third-order matrix elements to be larger than 1% for $Z < 10$.

For allowed transitions, the present calculations are found to be in excellent agreement with values from previous accurate calculations and with recommended values from the National Institute of Standards and Technology (NIST) [27] for all values of Z. We find, however, substantial differences between the present results and recommended values for forbidden transitions in ions with $Z < 10$, owing to the fact that we truncate the MBPT expansion at second order. We expect that accurate correlated CI, or R-matrix calculations for forbidden transitions will be superior to the present calculations for ions with $Z < 10$. However, for ions with $Z \geqslant 10$, we expect the present calculations for both allowed and forbidden transitions to be accurate to better than 1%, and, consequently, to be more accurate than available alternative calculations.

2. Method

In this section, we describe our application of MBPT to calculate transition amplitudes. Perhaps the only unusual feature of the present MBPT calculation is the appearance of the 'derivative' term

$$\delta k^{(1)} \frac{\mathrm{d}T^{(1)}}{\mathrm{d}k}$$

in the second-order matrix element. This term arises because the first-order transition amplitude $T^{(1)}(k)$ depends on the wavenumber $k = \omega/c$ of the transition, and k changes order-by-order in a MBPT calculation. Expressions for first-order matrix elements are identical to those used in recent CI calculations [24] for He-like ions. These expressions are repeated in the appendix.

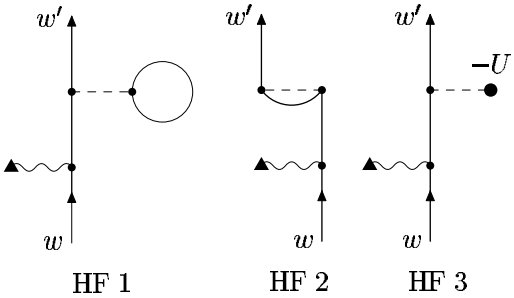

Figure 1. HF diagrams. The dashed lines designate Coulomb + Breit interactions and the wavy lines designate interactions with the dipole field. Diagrams HF1 and HF2 are direct and exchange contributions and HF3 is a counter-term that cancels with the first two when a HF starting potential $U(r) = V_{\mathrm{HF}}^{N-2}$ is used.

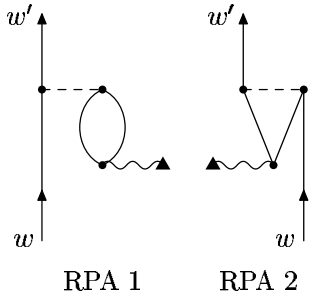

Figure 2. Random-phase approximation diagrams. Diagrams RPA1 and RPA2 are direct and exchange contributions. These diagrams account for the shielding of the dipole field by the core electrons.

The formalism developed in [25, 28] is used to obtain the perturbed wavefunctions needed in the second-order MBPT calculations. In the following section, we outline the second-order contributions to the transition matrix.

2.1. Second-order matrix elements

In this section, we discuss the various contributions to second-order transition matrix elements in terms of Bruckner–Goldstone diagrams. These diagrams can be divided into three subclasses: Hartree–Fock (HF) diagrams, random-phase approximation (RPA) diagrams, and correlation (corr) diagrams.

The HF diagrams are shown in figure 1. In MBPT calculations for systems with two valence electrons, a natural starting potential is a V_{HF}^{N-2} HF potential. For any other starting potential $U(r)$, an additional term of the form

$$\Delta V = \sum_{ij} [V_{\mathrm{HF}}^{N-2} - U]_{ij} a_i^{\dagger} a_j$$

appears in the interaction Hamiltonian. The HF diagrams give the second-order correction arising from one interaction with ΔV and one interaction with the transition operator. The panels labelled HF1 and HF2 in figure 1 give the contributions from the direct and exchange parts of the HF potential and the panel HF3 gives the contribution from the starting potential $U(r)$. Of course if we start our calculation using a HF potential, the three diagrams cancel

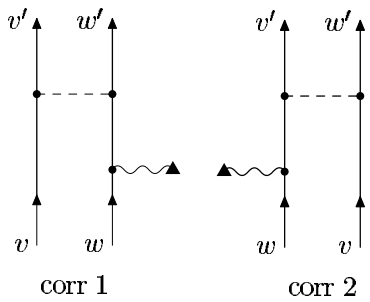

Figure 3. Correlation diagrams. Diagrams corr1 and corr2 are direct and exchange contributions. These diagrams correct the matrix element to account for interaction between the valence electrons.

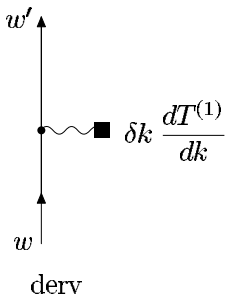

Figure 4. This diagram represents symbolically the second-order MBPT correction from the derivative term.

identically. When including the Breit interaction, care must be taken to include the Breit contributions to $V_{\rm HF}^{N-2}$. In the present calculation, we start our calculations using a Coulomb-only $1s^2$ HF potential. It follows that the Coulomb contributions to the diagrams in figure 1 cancel. However, the Breit contributions from the first two diagrams give non-vanishing contributions.

The RPA diagrams are illustrated in figure 2. These diagrams account in second-order for the shielding of the external dipole field by the atomic core orbitals. Exact (as contrasted to second-order) RPA matrix elements could be obtained by iterating the corresponding core RPA diagrams to all orders in perturbation theory. The exact RPA is used, for example, in [29] to study transitions in alkali-metal atoms.

In figure 3, the correlation diagrams are shown. These diagrams correct the first-order matrix elements for correlation between the valence electrons. Finally, in figure 4, we represent the contribution from the 'derivative' term diagrammatically.

Using the standard methods of MBPT laid out, for example, in [30], all of these second-order diagrams can be expressed as sums over intermediate single-particle states. Explicit formulae for the contributions from these diagrams, after an angular momentum reduction has been carried out, are given in the appendix.

2.2. Uncoupled matrix elements

In table 1, we list values of the first- and second-order dipole matrix elements $Z_1^{(1)}$, $Z_1^{(\rm RPA)}$, $Z_1^{(\rm corr)}$, and the matrix element of the derivative term $P_1^{(\rm derv)}$, for $J = 0$ to $J' = 1$ transitions in Be-like iron, $Z = 26$. (The subscripts '1' on the above symbols designate electric-dipole matrix elements.) Both length and velocity forms of the matrix elements are given. The Coulomb HF contribution $Z_1^{(\rm HF)}$ vanishes in the present calculation since we use HF basis functions. We use the symbol B in table 1 to denote the Breit contributions to the second-order

Table 1. Uncoupled reduced matrix elements in length (L) and velocity (V) forms for Fe^{22+}. Notation: $np = np_{3/2}$, $np^* = np_{1/2}$ $3d = 3d_{5/2}$, $3d^* = 3d_{3/2}$.

Coulomb interaction						
$vw[J]$	$v'w'[J']$		$Z_1^{(1)}$	$P_1^{(\mathrm{derv})}$	$Z_1^{(\mathrm{RPA})}$	$Z_1^{(\mathrm{corr})}$
2s2s[0]	2s3p*[1]	(L)	0.094 712	0.094 468	0.000 078	−0.000 513
		(V)	0.094 358	−0.000 014	0.000 418	−0.003 803
2s2s[0]	2s3p[1]	(L)	−0.130 829	−0.130 256	−0.000 109	0.000 788
		(V)	−0.130 330	0.000 473	−0.000 589	0.005 347
2p*2p*[0]	2p*3s[1]	(L)	0.035 475	0.035 263	0.000 120	0.003 442
		(V)	0.035 815	−0.000 144	−0.000 215	0.000 989
2p*2p*[0]	2p*3d*[1]	(L)	0.220 722	0.220 316	−0.000 223	0.001 964
		(V)	0.220 597	−0.000 264	−0.000 094	−0.007 747
2p2p[0]	2p3s[1]	(L)	0.037 336	0.037 182	0.000 117	0.004 899
		(V)	0.037 680	−0.000 027	−0.000 221	0.001 970
2p2p[0]	2p3d*[1]	(L)	−0.070 823	−0.070 810	0.000 070	−0.000 372
		(V)	−0.070 783	−0.000 147	0.000 029	0.003 194
2p2p[0]	2p3d[1]	(L)	0.212 097	0.211 483	−0.000 210	0.002 904
		(V)	0.211 977	−0.000 709	−0.000 087	−0.007 878
2s2s[0]	2p3d[1]	(L)	0.000 000	0.000 000	0.000 000	−0.003 335
		(V)	0.000 000	0.000 000	0.000 000	0.000 824
2p*2p*[0]	2s3p*[1]	(L)	0.000 000	0.000 000	0.000 000	−0.002 417
		(V)	0.000 000	0.000 000	0.000 000	−0.001 745

Breit interaction with factor 10^3						
$vw[J]$	$v'w'[J']$		$B_1^{(\mathrm{HF})}$	$B_1^{(\mathrm{RPA})}$	$B_1^{(\mathrm{corr})}$	$B_1^{(2)}$
2s2s[0]	2s3p ∗ [1]	(L)	−0.053 496	0.003 206	0.020 739	−0.029 551
		(V)	−0.054 252	−0.018 166	0.008 712	−0.063 706
2s2s[0]	2s3p[1]	(L)	−0.035 893	−0.001 489	−0.021 881	−0.059 263
		(V)	−0.002 582	0.015 172	−0.008 793	0.003 796
2p*2p*[0]	2p*3s[1]	(L)	0.076 405	0.002 662	0.035 957	0.115 025
		(V)	0.026 105	0.022 590	0.022 874	0.071 569
2p*2p*[0]	2p*3d*[1]	(L)	0.214 353	−0.001 696	0.019 028	0.231 685
		(V)	0.015 581	−0.017 973	−0.022 762	−0.025 154
2p2p[0]	2p3s[1]	(L)	0.008 886	0.000 055	0.060 090	0.069 030
		(V)	−0.012 661	0.010 643	0.037 731	0.035 714
2p2p[0]	2p3d*[1]	(L)	−0.030 222	−0.000 373	−0.019 089	−0.049 684
		(V)	−0.002 535	0.004 366	0.011 825	0.013 656
2p2p[0]	2p3d[1]	(L)	0.093 410	−0.000 732	0.031 977	0.124 655
		(V)	0.006 030	−0.009 410	−0.035 537	−0.038 917
2s2s[0]	2p3d[1]	(L)	0.000 000	0.000 000	−0.031 536	−0.031 536
		(V)	0.000 000	0.000 000	−0.002 369	−0.002 369
2p*2p*[0]	2s3p*[1]	(L)	0.000 000	0.000 000	−0.027 722	−0.027 722
		(V)	0.000 000	0.000 000	−0.018 586	−0.018 586

matrix elements, and we tabulate 1000 times $B^{(\mathrm{HF})}$, $B^{(\mathrm{RPA})}$, $B^{(\mathrm{corr})}$, and the sum $B^{(2)}$. As can be seen from the table, the first-order contributions $Z_1^{(1)}$ are different in length and velocity forms. One also observes that the total second-order Breit corrections $B_1^{(2)}$ are smaller than the RPA terms $Z_1^{(\mathrm{RPA})}$, and that these RPA corrections are smaller than the correlation corrections $Z_1^{(\mathrm{corr})}$. The ratios between these terms change with nuclear charge.

Table 2. Coupled reduced matrix elements Q calculated in length (L) and velocity (V) forms for Fe^{22+}.

$l_1 l_2\ LSJ$	$l_3 l_4\ L'S'J'$	L	V	$j_1 j_2\ [J]$	$j_3 j_4\ [J']$
$2s^2\ ^1S_0$	$2s3p\ ^1P_1$	0.096 683	0.096 679	2s2s[0]	2s3p*[1]
$2s^2\ ^1S_0$	$2s3p\ ^3P_1$	0.121 971	0.121 965	2s2s[0]	2s3p[1]
$2s^2\ ^1S_0$	$2p3s\ ^3P_1$	0.021 220	0.021 219	2s2s[0]	2p*3s[1]
$2s^2\ ^1S_0$	$2p3s\ ^1P_1$	0.028 059	0.028 058	2s2s[0]	2p3s[1]
$2s^2\ ^1S_0$	$2p3d\ ^3D_1$	0.013 741	0.013 729	2s2s[0]	2p*3d*[1]
$2s^2\ ^1S_0$	$2p3d\ ^3P_1$	0.002 652	0.002 649	2s2s[0]	2p3d*[1]
$2s^2\ ^1S_0$	$2p3d\ ^1P_1$	0.025 554	0.025 522	2s2s[0]	2p3d[1]
$2p^2\ ^3P_0$	$2s3p\ ^1P_1$	0.005 073	0.005 076	2p*2p*[0]	2s3p*[1]
$2p^2\ ^3P_0$	$2s3p\ ^3P_1$	0.005 175	0.005 173	2p*2p*[0]	2s3p[1]
$2p^2\ ^3P_0$	$2p3s\ ^3P_1$	0.049 130	0.049 129	2p*2p*[0]	2p*3s[1]
$2p^2\ ^3P_0$	$2p3s\ ^1P_1$	0.009 862	0.009 859	2p*2p*[0]	2p3s[1]
$2p^2\ ^3P_0$	$2p3d\ ^3D_1$	0.217 524	0.217 536	2p*2p*[0]	2p*3d*[1]
$2p^2\ ^3P_0$	$2p3d\ ^3P_1$	0.008 938	0.008 940	2p*2p*[0]	2p3d*[1]
$2p^2\ ^3P_0$	$2p3d\ ^1P_1$	0.030 138	0.030 138	2p*2p*[0]	2p3d[1]
$2p^2\ ^1S_0$	$2s3p\ ^1P_1$	0.005 824	0.005 814	2p2p[0]	2s3p*[1]
$2p^2\ ^1S_0$	$2s3p\ ^3P_1$	0.003 701	0.003 687	2p2p[0]	2s3p[1]
$2p^2\ ^1S_0$	$2p3s\ ^3P_1$	0.009 104	0.009 107	2p2p[0]	2p*3s[1]
$2p^2\ ^1S_0$	$2p3s\ ^1P_1$	0.050 961	0.050 971	2p2p[0]	2p3s[1]
$2p^2\ ^1S_0$	$2p3d\ ^3D_1$	0.029 345	0.029 347	2p2p[0]	2p*3d*[1]
$2p^2\ ^1S_0$	$2p3d\ ^3P_1$	0.019 784	0.019 785	2p2p[0]	2p3d*[1]
$2p^2\ ^1S_0$	$2p3d\ ^1P_1$	0.221 952	0.221 967	2p2p[0]	2p3d[1]
$2p^2\ ^3P_1$	$2s3p\ ^1P_1$	0.004 883	0.004 884	2p*2p[1]	2s3p*[1]
$2p^2\ ^3P_1$	$2s3p\ ^3P_1$	0.001 655	0.001 656	2p*2p[1]	2s3p[1]
$2p^2\ ^3P_1$	$2p3s\ ^3P_1$	0.036 948	0.036 947	2p*2p[1]	2p*3s[1]
$2p^2\ ^3P_1$	$2p3s\ ^1P_1$	0.015 894	0.015 894	2p*2p[1]	2p3s[1]
$2p^2\ ^3P_1$	$2p3d\ ^3D_1$	0.101 606	0.101 611	2p*2p[1]	2p*3d*[1]
$2p^2\ ^3P_1$	$2p3d\ ^3P_1$	0.160 329	0.160 338	2p*2p[1]	2p3d*[1]
$2p^2\ ^3P_1$	$2p3d\ ^1P_1$	0.023 265	0.023 266	2p*2p[1]	2p3d[1]
$2p^2\ ^3P_2$	$2s3p\ ^1P_1$	0.016 235	0.016 244	2p*2p[2]	2s3p*[1]
$2p^2\ ^3P_2$	$2s3p\ ^3P_1$	0.012 072	0.012 081	2p*2p[2]	2s3p[1]
$2p^2\ ^3P_2$	$2p3s\ ^3P_1$	0.058 686	0.058 680	2p*2p[2]	2p*3s[1]
$2p^2\ ^3P_2$	$2p3s\ ^1P_1$	0.015 596	0.015 586	2p*2p[2]	2p3s[1]
$2p^2\ ^3P_2$	$2p3d\ ^3D_1$	0.020 916	0.020 908	2p*2p[2]	2p*3d*[1]
$2p^2\ ^3P_2$	$2p3d\ ^3P_1$	0.113 174	0.113 178	2p*2p[2]	2p3d*[1]
$2p^2\ ^3P_2$	$2p3d\ ^1P_1$	0.006 002	0.005 980	2p*2p[2]	2p3d[1]
$2p^2\ ^1D_2$	$2s3p\ ^1P_1$	0.013 540	0.013 555	2p2p[2]	2s3p*[1]
$2p^2\ ^1D_2$	$2s3p\ ^3P_1$	0.025 856	0.025 875	2p2p[2]	2s3p[1]
$2p^2\ ^1D_2$	$2p3s\ ^3P_1$	0.002 649	0.002 641	2p2p[2]	2p*3s[1]
$2p^2\ ^1D_2$	$2p3s\ ^1P_1$	0.077 184	0.077 167	2p2p[2]	2p3s[1]
$2p^2\ ^1D_2$	$2p3d\ ^3D_1$	0.009 827	0.009 811	2p2p[2]	2p*3d*[1]
$2p^2\ ^1D_2$	$2p3d\ ^3P_1$	0.058 079	0.058 085	2p2p[2]	2p3d*[1]

2.3. Coupled matrix elements

As mentioned in the introduction, physical two-particle states are linear combinations of uncoupled two-particle states. For the Fe^{22+} example discussed above, the transition amplitudes between physical states are linear combinations of the uncoupled transition matrix elements given in table 1. The expansion coefficients and energies are obtained by diagonalizing the first-order effective Hamiltonian which includes both Coulomb and Breit interactions. We

Table 3. Contributions to the coupled reduced matrix elements in length L and velocity V forms for the 2s2p ^{3}P$_2$–2p3p ^{3}D$_3$ and 2s2p ^{3}P$_2$–2s3d ^{3}D$_3$ transitions in Fe^{+22}. Coulomb potential: $\varepsilon_{2s2p} - \varepsilon_{2s3d} = -47.097\,7901$, $\varepsilon_{2s2p} - \varepsilon_{2p3p} = -47.799\,9452$, E_1^I–$E_1^{F1} = -39.619\,8519$, E_1^I–$E_1^{F2} = 41.586\,3816$ and Dirac–Fock potential: $\varepsilon_{2s2p} - \varepsilon_{2s3d} = -40.777\,9346$, $\varepsilon_{2s2p} - \varepsilon_{2p3p} = -42.930\,9375$, E_1^I–$E_1^{F1} = -39.811\,914\,59$, E_1^I–$E_1^{F2} = -41.713\,117\,49$; I = 2s2p ^{3}P$_2$, F_1 = 2s3d ^{3}D$_3$, F_2 = 2p3p ^{3}D$_3$.

	2s2p$_{3/2}$[2]–2s3d$_{5/2}$[3]		2s2p$_{3/2}$[2]–2p$_{3/2}$3p$_{3/2}$[3]	
	L	V	L	V
Coulomb potential				
$Z^{(1)}$	0.303 8452	0.303 8452	0.174 4182	0.174 4182
$Z^{(\mathrm{HF})}$	0.018 3226	−0.023 6117	−0.000 8382	−0.019 4827
$Z^{(\mathrm{RPA})}$	−0.000 3507	−0.000 1567	0.000 1350	0.000 7842
$Z^{(\mathrm{corr})}$	0.000 2679	−0.006 6715	−0.000 9389	−0.006 7626
$B^{(\mathrm{HF})}$	0.000 1353	0.000 006 9	0.000 048 7	0.000 0048
$B^{(\mathrm{RPA})}$	−0.000 0013	−0.000 0138	0.000 0024	−0.000 0178
$B^{(\mathrm{corr})}$	0.000 0216	0.000 001 8	−0.000 0018	−0.000 0168
$(Z + B)$	0.322 2405	0.273 4001	0.172 8255	0.148 9272
$P^{(\mathrm{derv})}$	0.302 8330	−0.001 1717	0.173 5980	−0.000 6874
Q^{F_1}	0.325 9034	0.325 2234	0.172 6660	0.179 8174
Q^{F_2}	0.324 8125	0.309 7889	0.172 7101	0.171 2817
C^{F_1}	0.995 5104	0.995 5104	0.094 6523	0.094 6523
C^{F_2}	−0.094 6523	−0.094 6523	0.995 5104	0.995 5104
$Q(I–F)$	0.340 7835	0.340 7834	0.141 1904	0.141 1905
Dirac–Fock potential				
$Z^{(1)}$	0.323 9842	0.323 8003	0.173 0699	0.172 4109
$Z^{(\mathrm{HF})}$	0	0	0	0
$Z^{(\mathrm{RPA})}$	−0.000 3204	−0.000 1329	0.000 1436	0.000 7788
$Z^{(\mathrm{corr})}$	0.000 2326	−0.007 8991	−0.001 2800	−0.007 5426
$B^{(\mathrm{HF})}$	0.000 1427	0.000 0092	0.000 0475	0.000 0034
$B^{(\mathrm{RPA})}$	−0.000 0011	−0.000 0144	0.000 0020	−0.000 0201
$B^{(\mathrm{corr})}$	0.000 0194	0.000 0010	0.000 0008	−0.000 0123
$(Z + B)$	0.324 0573	0.315 7641	0.171 9837	0.165 6181
$P^{(\mathrm{derv})}$	0.323 046 0	−0.001 0837	0.172 3129	−0.000 6255
Q^{F_1}	0.324 0819	0.323 4523	0.171 9579	0.178 6423
Q^{F_2}	0.324 0347	0.308 6606	0.171 9741	0.170 4716
C^{F_1}	0.995 3417	0.995 3417	0.096 4101	0.096 4101
C^{F_2}	−0.096 4101	−0.096 4101	0.995 3417	0.995 3417
$Q(I–F)$	0.339 1507	0.339 1685	0.139 9328	0.139 9195

let $C_1^\lambda(vw)$ designate the λth eigenvector of the first-order effective Hamiltonian and let E_1^λ be the corresponding eigenvalue. The coupled transition matrix element between the initial eigenstate I with angular momentum J and the final state F with angular momentum J' is given by:

$$\begin{aligned} Q^{(1+2)}(I-F) = {} & \frac{1}{E_1^I - E_1^F} \sum_{vw} \sum_{v'w'} C_1^I(vw) C_1^F(v'w') \\ & \times \{[\varepsilon_{vw} - \varepsilon_{v'w'}][Z_1^{(1+2)}[vw(J)–v'w'(J')] + B_1^{(2)}[vw(J)–v'w'(J')]] \\ & + [E_1^I - E_1^F - \varepsilon_{vw} + \varepsilon_{v'w'}] P_1^{(\mathrm{derv})}[vw(J)–v'w'(J')]\}. \end{aligned} \tag{2.1}$$

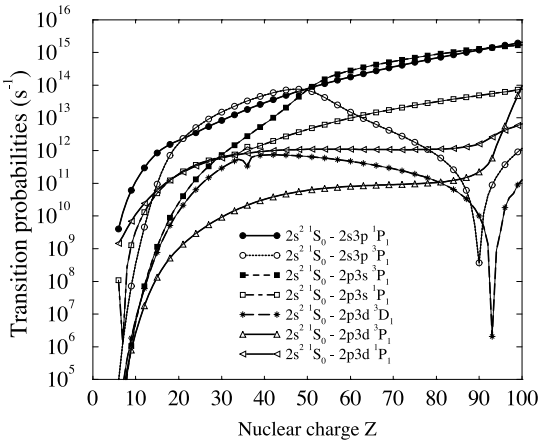

Figure 5. Transition probabilities $A(2\mathrm{s}^2\,{}^1\mathrm{S}_0$–$2l3l'\,{}^{2S+1}L_1)$ as functions of Z.

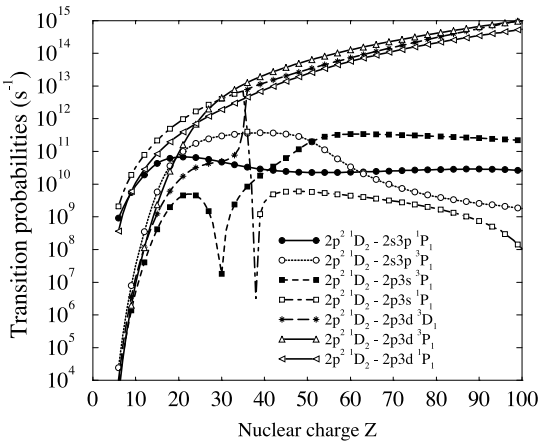

Figure 6. Transition probabilities $A(2\mathrm{p}^2\,{}^1\mathrm{D}_2$–$2l3l'\,{}^{2S+1}L_1)$ as functions of Z.

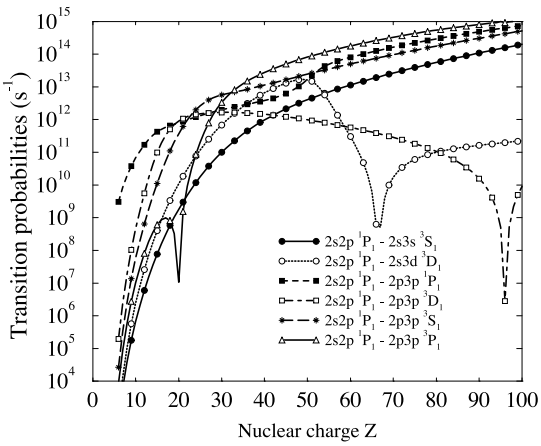

Figure 7. Transition probabilities $A(2\mathrm{s}2\mathrm{p}\,{}^1\mathrm{P}_1$–$2l3l'\,{}^{2S+1}L_1)$ as functions of Z.

Here $\varepsilon_{vw} = \varepsilon_v + \varepsilon_w$ and $Z_1^{(1+2)} = Z_1^{(1)} + Z_1^{(\mathrm{HF})} + Z_1^{(\mathrm{RPA})} + Z_1^{(\mathrm{corr})}$. Using these formulae together with the uncoupled reduced matrix elements given in table 1, we transform the uncoupled matrix elements to matrix elements between coupled (physical) states. In table 2, we present values of the 16 $2l_1 2l_2[LSJ]$–$2l_3 3l_4[L'S'J']$ coupled reduced matrix elements Q in length

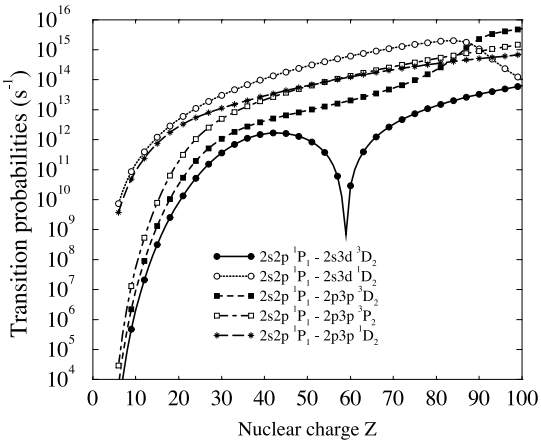

Figure 8. Transition probabilities $A(2\mathrm{s}2\mathrm{p}\,^1\mathrm{P}_1$–$2l3l'\,^{2S+1}L_2)$ as functions of Z.

(L) and velocity (V) forms for Be-like iron, $Z = 26$. Even though the results are obtained in intermediate coupling, it is, nevertheless, convenient to label the physical states using the $[LSJ]$ scheme. We can see that the results obtained in the L and V forms differ only in the fourth or fifth significant figures except for the intercombination transitions $2\mathrm{p}^2\,^1\mathrm{S}_0$–$2\mathrm{s}3\mathrm{p}\,^3\mathrm{P}_1$, $2\mathrm{p}^2\,^3\mathrm{P}_2$–$2\mathrm{p}3\mathrm{d}\,^1\mathrm{P}_1$, $2\mathrm{p}^2\,^1\mathrm{D}_2$–$2\mathrm{p}3\mathrm{s}\,^3\mathrm{P}_1$, and $2\mathrm{p}^2\,^1\mathrm{D}_2$–$2\mathrm{p}3\mathrm{d}\,^3\mathrm{D}_1$, all of which are relatively small.

As mentioned previously, these $L - V$ differences arise because we start our calculations using the non-local HF potential. It was shown for He-like ions in [24] that first- and second-order MBPT matrix elements are gauge-independent for calculations starting from a *local* potential. The arguments of [24] are easily extended to Be-like ions. Let us demonstrate the gauge independence for the transitions $2\mathrm{s}2\mathrm{p}\,^3\mathrm{P}_2$–$2\mathrm{s}3\mathrm{d}\,^3\mathrm{D}_3$ and $2\mathrm{s}2\mathrm{p}\,^3\mathrm{P}_2$–$2\mathrm{p}3\mathrm{p}\,^3\mathrm{D}_3$. Here the initial state $I = 2\mathrm{s}2\mathrm{p}\,^3\mathrm{P}_2 \equiv 2\mathrm{s}2\mathrm{p}_{3/2}(2)$ is a single-configuration state in any coupling scheme and only the final states are mixed. Using the $[LSJ]$ designation for coupled states $F_1 = 2\mathrm{s}3\mathrm{d}\,^3\mathrm{D}_3$ and $F_2 = 2\mathrm{p}3\mathrm{p}\,^3\mathrm{D}_3$ and the $[jjJ]$ designation for uncoupled states $2\mathrm{s}3\mathrm{d}_{3/2}(3)$ and $2\mathrm{p}_{3/2}3\mathrm{p}_{3/2}(3)$, we can rewrite $Q^{(1+2)}[I\text{–}F_k]$ (k distinguishes the two possible final states) in the following way:

$$Q^{(1+2)}[I\text{–}F_k] = C_1^{F_k}(2\mathrm{s}3\mathrm{d}_{3/2}(3))\, Q^{F_k}[I\text{–}2\mathrm{s}3\mathrm{d}_{5/2}(3)] + C_1^{F_k}(2\mathrm{p}_{3/2}3\mathrm{p}_{3/2}(3))\, Q^{F_k}[I\text{–}2\mathrm{p}_{3/2}3\mathrm{p}_{3/2}(3)], \tag{2.2}$$

where

$$Q^{F_k}[I\text{–}2\mathrm{s}3\mathrm{d}_{5/2}(3)] = \frac{\varepsilon_{2\mathrm{p}_{3/2}} - \varepsilon_{3\mathrm{d}_{5/2}}}{E_1^I - E_1^{F_k}} \left\{ (Z^{(1+2)} + B^{(2)})[2\mathrm{s}2\mathrm{p}_{3/2}(2)\text{–}2\mathrm{s}3\mathrm{d}_{5/2}(3)] + \left(1 - \frac{\varepsilon_{2\mathrm{p}_{3/2}} - \varepsilon_{3\mathrm{d}_{5/2}}}{E_1^I - E_1^{F_k}}\right) P^{(\mathrm{derv})}[2\mathrm{s}2\mathrm{p}_{3/2}(2)\text{–}2\mathrm{s}3\mathrm{d}_{5/2}(3)] \right\}, \tag{2.3}$$

$$Q^{F_k}[I\text{–}2\mathrm{p}_{3/2}3\mathrm{p}_{3/2}(3)] = \frac{\varepsilon_{2\mathrm{s}} - \varepsilon_{3\mathrm{p}_{3/2}}}{E_1^I - E_1^{F_k}} \left\{ (Z^{(1+2)} + B^{(2)})[2\mathrm{s}2\mathrm{p}_{3/2}(2)\text{–}2\mathrm{p}_{3/2}3\mathrm{p}_{3/2}(3)] + \left(1 - \frac{\varepsilon_{2\mathrm{s}} - \varepsilon_{3\mathrm{p}_{3/2}}}{E_1^I - E_1^{F_k}}\right) P^{(\mathrm{derv})}[2\mathrm{s}2\mathrm{p}_{3/2}(2)\text{–}2\mathrm{p}_{3/2}3\mathrm{p}_{3/2}(3)] \right\}. \tag{2.4}$$

We list the individual contributions to this transition for Be-like iron in table 3. In the first two columns, we compare results obtained with the local Coulomb potential in L and V forms. We see that the first-order results are identical in the two forms to the figures quoted even for uncoupled matrix elements. The second-order uncoupled matrix elements $Q^{F_1}[I\text{–}2\mathrm{s}3\mathrm{d}_{5/2}(3)]$,

Table 4. Wavelengths λ (Å), transition rates A (s^{-1}), oscillator strengths f, and line strengths S (au) for even–odd transitions in Be-like nitrogen and oxygen. a: present result, b: recommended values [27].

			$Z = 7$				$Z = 8$			
$l_1l_2\ LSJ$	$l_3l_4\ L'S'J'$		λ	A	f	S	λ	A	f	S
$2s^2\,{}^1S_0$	$2s3p\,{}^1P_1$	a	247.133	1.24(10)	3.41(−1)	2.77(−1)	172.158	2.96(10)	3.95(−1)	2.24(−1)
		b		1.19(10)	3.27(−1)	2.66(−1)		2.94(10)	3.92(−1)	2.22(−1)
$2p^2\,{}^3P_2$	$2p3d\,{}^3P_2$	a	299.550	1.51(10)	2.03(−1)	1.00(0)	201.960	3.52(10)	2.15(−1)	7.16(−1)
		b		1.05(10)	1.39(−1)	6.82(−1)		3.43(10)	2.11(−1)	7.02(−1)
$2p^2\,{}^3P_1$	$2p3d\,{}^3P_1$	a	299.368	5.15(09)	6.93(−2)	2.05(−1)	201.788	1.22(10)	7.47(−2)	1.49(−1)
		b		3.49(09)	4.64(−2)	1.36(−1)		1.21(10)	7.39(−2)	1.48(−1)
$2p^2\,{}^3P_2$	$2p3d\,{}^3P_1$	a	299.482	8.18(09)	6.61(−2)	3.26(−1)	201.899	1.88(10)	6.88(−2)	2.29(−1)
		b		5.81(09)	4.64(−2)	2.27(−1)		1.81(10)	6.68(−2)	2.22(−1)
$2p^2\,{}^3P_1$	$2p3d\,{}^3P_0$	a	299.334	1.94(10)	8.70(−2)	2.57(−1)	201.756	4.42(10)	8.99(−2)	1.79(−1)
		b		1.40(10)	6.18(−2)	1.82(−1)		4.25(10)	8.69(−2)	1.74(−1)
$2p^2\,{}^3P_1$	$2p3d\,{}^3P_2$	a	299.435	4.32(09)	9.68(−2)	2.86(−1)	201.849	8.95(09)	9.11(−2)	1.82(−1)
		b		3.49(09)	7.73(−2)	2.27(−1)		8.18(09)	8.37(−2)	1.67(−1)
$2p^2\,{}^3P_0$	$2p3d\,{}^3P_1$	a	299.301	6.08(09)	2.45(−1)	2.42(−1)	201.724	1.32(10)	2.42(−1)	1.60(−1)
		b		4.66(09)	1.86(−1)	1.82(−1)		1.23(10)	2.27(−1)	1.51(−1)
$2p^2\,{}^3P_2$	$2p3d\,{}^3D_3$	a	302.610	3.61(10)	6.93(−1)	3.45(0)	203.690	8.26(10)	7.20(−1)	2.41(0)
		b		3.49(10)	6.72(−1)	3.35(0)		8.16(10)	7.12(−1)	2.39(0)
$2p^2\,{}^3P_1$	$2p3d\,{}^3D_2$	a	302.537	2.76(10)	6.31(−1)	1.88(0)	203.621	6.40(10)	6.64(−1)	1.33(0)
		b		2.62(10)	6.10(−1)	1.80(0)		6.36(10)	6.60(−1)	1.33(0)
$2p^2\,{}^3P_0$	$2p3d\,{}^3D_1$	a	302.497	2.04(10)	8.41(−1)	8.38(−1)	203.584	4.74(10)	8.84(−1)	5.92(−1)
		b		1.94(10)	8.01(−1)	7.99(−1)		4.71(10)	8.80(−1)	5.90(−1)
$2p^2\,{}^3P_2$	$2p3d\,{}^3D_2$	a	302.654	8.48(09)	1.17(−1)	5.81(−1)	203.734	1.85(10)	1.15(−1)	3.87(−1)
		b		8.71(09)	1.20(−1)	5.99(−1)		1.79(10)	1.12(−1)	3.74(−1)
$2p^2\,{}^3P_1$	$2p3d\,{}^3D_1$	a	302.565	1.47(10)	2.02(−1)	6.05(−1)	203.649	3.32(10)	2.07(−1)	4.16(−1)
		b		1.45(10)	2.00(−1)	5.99(−1)		3.26(10)	2.03(−1)	4.09(−1)
$2p^2\,{}^3P_2$	$2p3d\,{}^3D_1$	a	302.682	9.06(08)	7.47(−3)	3.72(−2)	203.762	1.92(09)	7.19(−3)	2.41(−2)
		b		9.68(08)	8.00(−3)	3.99(−2)		1.83(09)	6.84(−3)	2.30(−2)
$2p^2\,{}^3P_2$	$2p3s\,{}^3P_2$	a	344.511	5.43(09)	9.66(−2)	5.48(−1)	227.304	1.10(10)	8.54(−2)	3.19(−1)
		b		4.94(09)	8.81(−2)	5.00(−1)		1.03(10)	8.02(−2)	3.00(−1)
$2p^2\,{}^3P_1$	$2p3s\,{}^3P_1$	a	344.557	1.80(09)	3.21(−2)	1.09(−1)	227.341	3.66(09)	2.83(−2)	6.37(−2)
		b		1.64(09)	2.94(−2)	1.00(−1)		3.42(09)	2.65(−2)	5.97(−2)
$2p^2\,{}^3P_2$	$2p3s\,{}^3P_1$	a	344.709	3.01(09)	3.22(−2)	1.83(−1)	227.482	6.11(09)	2.85(−2)	1.07(−1)
		b		2.74(09)	2.94(−2)	1.67(−1)		5.72(09)	2.67(−2)	9.99(−2)
$2p^2\,{}^3P_1$	$2p3s\,{}^3P_0$	a	344.651	7.22(09)	4.29(−2)	1.46(−1)	227.425	1.46(10)	3.79(−2)	8.51(−2)
		b		6.57(09)	3.91(−2)	1.33(−1)		1.37(10)	3.55(−2)	7.99(−2)
$2p^2\,{}^3P_1$	$2p3s\,{}^3P_2$	a	344.359	1.81(09)	5.38(−2)	1.83(−1)	227.163	3.68(09)	4.76(−2)	1.07(−1)
		b		1.65(09)	4.90(−2)	1.67(−1)		3.46(09)	4.47(−2)	1.00(−1)
$2p^2\,{}^3P_0$	$2p3s\,{}^3P_1$	a	344.469	2.41(09)	1.29(−1)	1.46(−1)	227.260	4.90(09)	1.14(−1)	8.51(−2)
		b		2.19(09)	1.17(−1)	1.33(−1)		4.58(09)	1.07(−1)	7.99(−2)
$2p^2\,{}^3P_2$	$2s3p\,{}^3P_2$	a	433.025	1.11(07)	3.12(−4)	2.23(−3)	270.601	4.63(07)	5.09(−4)	2.27(−3)
		b		1.13(07)	3.21(−4)	2.29(−3)		4.24(07)	4.66(−4)	2.08(−3)
$2p^2\,{}^3P_1$	$2s3p\,{}^3P_1$	a	432.851	3.66(06)	1.03(−4)	4.40(−4)	270.458	1.52(07)	1.66(−4)	4.45(−4)
		b		3.78(06)	1.07(−4)	4.58(−4)		1.38(07)	1.52(−4)	4.06(−4)
$2p^2\,{}^3P_2$	$2s3p\,{}^3P_1$	a	433.091	6.15(06)	1.04(−4)	7.40(−4)	270.658	2.54(07)	1.68(−4)	7.48(−4)
		b		6.30(06)	1.07(−4)	7.64(−4)		2.31(07)	1.53(−4)	6.81(−4)
$2p^2\,{}^3P_1$	$2s3p\,{}^3P_0$	a	432.881	1.48(07)	1.38(−4)	5.92(−4)	270.485	6.12(07)	2.24(−4)	5.99(−4)
		b		1.57(07)	1.43(−4)	6.11(−4)		5.57(07)	2.04(−4)	5.47(−4)
$2p^2\,{}^3P_1$	$2s3p\,{}^3P_2$	a	432.786	3.74(06)	1.75(−4)	7.49(−4)	270.402	1.56(07)	2.86(−4)	7.65(−4)
		b		3.79(06)	1.78(−4)	7.64(−4)		1.44(07)	2.65(−4)	7.08(−4)

Table 4. (Continued)

			$Z = 7$				$Z = 8$			
$l_1 l_2\ LSJ$	$l_3 l_4\ L'S'J'$		λ	A	f	S	λ	A	f	S
$2p^2\ ^3P_0$	$2s3p\ ^3P_1$	a	432.713	4.95(06)	4.17(−4)	5.94(−4)	270.344	2.06(07)	6.77(−4)	6.03(−4)
		b		5.05(06)	4.28(−4)	6.11(−4)		1.88(07)	6.21(−4)	5.53(−4)
$2p^2\ ^1D_2$	$2p3d\ ^1P_1$	a	303.015	1.22(09)	1.02(−2)	5.02(−2)	204.164	2.95(09)	1.11(−2)	3.72(−2)
		b		8.72(08)	7.21(−3)	3.60(−2)		2.26(09)	8.56(−2)	2.89(−2)
$2p^2\ ^1D_2$	$2p3d\ ^1F_3$	a	311.588	3.43(10)	6.99(−1)	3.59(0)	207.747	8.56(10)	7.76(−1)	2.65(0)
		b		1.36(10)	2.84(−1)	1.47(0)		8.58(10)	7.78(−1)	2.66(0)
$2p^2\ ^1D_2$	$2p3d\ ^1D_2$	a	320.658	4.75(10)	7.33(−2)	3.87(−1)	215.075	1.90(10)	1.32(−1)	4.67(−1)
		b		1.40(10)	2.20(−1)	1.17(0)		3.07(10)	2.15(−1)	7.64(−1)
$2p^2\ ^1S_1$	$2p3d\ ^1P_1$	a	352.873	2.16(10)	1.20(0)	1.41(0)	230.651	5.08(10)	1.22(0)	9.24(−1)
		b		1.80(10)	1.01(0)	1.17(0)		4.36(10)	1.05(0)	8.05(−1)
$2p^2\ ^1D_2$	$2p3s\ ^1P_1$	a	350.161	5.11(09)	5.64(−2)	3.25(−1)	230.570	1.05(10)	5.03(−2)	1.91(−1)
		b		5.33(09)	5.94(−2)	3.44(−1)		1.12(10)	5.37(−2)	2.04(−1)
$2p^2\ ^1S_0$	$2p3s\ ^1P_1$	a	418.489	1.82(09)	1.44(−1)	1.98(−1)	264.928	3.87(09)	1.22(−1)	1.07(−1)
		b		1.99(09)	1.59(−1)	2.20(−1)		4.39(09)	1.39(−1)	1.22(−1)
$2p^2\ ^1D_2$	$2s3p\ ^1P_1$	a	458.975	1.79(09)	3.39(−2)	2.56(−1)	285.014	3.28(09)	2.40(−2)	1.12(−1)
		b		1.06(09)	2.04(−2)	1.56(−1)		2.28(09)	1.68(−2)	7.94(−2)
$2p^2\ ^1S_0$	$2s3p\ ^1P_1$	a	583.947	3.89(07)	5.97(−3)	1.15(−2)	339.428	7.01(07)	3.63(−3)	4.06(−3)
		b		6.67(07)	1.05(−2)	2.04(−2)		1.26(08)	6.63(−3)	7.42(−3)
$2s^2\ ^1S_0$	$2s3p\ ^3P_1$	a	246.174	1.33(06)	3.63(−5)	2.95(−5)	171.512	1.17(07)	1.56(−4)	8.78(−5)
		b		3.08(06)	8.39(−5)	6.81(−5)				
$2s^2\ ^1S_0$	$2p3s\ ^1P_1$	a	211.709	1.26(06)	2.54(−5)	1.77(−5)	150.668	2.72(08)	2.78(−3)	1.38(−3)
		b		2.22(08)	4.45(−3)	3.10(−3)				
$2s^2\ ^1S_0$	$2p3d\ ^1P_1$	a	193.506	2.35(09)	3.96(−2)	2.32(−2)	138.927	4.12(09)	3.58(−2)	1.64(−2)
		b		3.58(08)	5.99(−3)	3.80(−3)		5.13(09)	4.46(−2)	2.04(−2)

$Q^{F_1}[I\text{–}2p_{3/2}3p_{3/2}(3)]$ and $Q^{F_2}[I\text{–}2s3d_{5/2}(3)]$, $Q^{F_2}[I\text{–}2p_{3/2}3p_{3/2}(3)]$ are different in the two gauges but, for the Coulomb case, they become identical after coupling. Thus for the local Coulomb potential, both first- and second-order matrix elements are identical in L and V forms. We do not obtain exact agreement between L and V forms for calculations starting from the non-local HF. However, as seen in the final row of table 3, the $L - V$ differences are very small for the final coupled matrix element even in the HF case. The largest $L - V$ differences occur for forbidden transitions. They range between 0.1% and 1% for the transitions shown in table 2 and are smaller than the uncertainties in available experimental data.

2.4. Negative-energy contributions

Negative-energy state (NES) contributions to the second-order reduced matrix element arise from terms in the sums over states i and n in equations (A3)–(A5) for which $\varepsilon_i < -mc^2$. The NES contributions for non-relativistically allowed transitions were discussed in [24] for He-like ions, where they were found to be most important for velocity-form matrix elements; they do not significantly modify length-form matrix elements. Also, it was shown in [24] that the inclusion of NES is necessary to insure gauge independence. We confirm this conclusion for Be-like ions here. The matrix elements in tables 1–3 include NES contributions. In [31], it was shown that NES contributions can be comparable to the 'regular' positive-energy contributions for certain non-relativistically forbidden transitions in He-like ions. We observed similar large contributions here for LS-forbidden transitions.

Table 5. Wavelengths λ (Å), transition rates A (s^{-1}), oscillator strengths f, and line strengths S (au) for odd–even transitions in Be-like nitrogen and oxygen. a: present result, b: recommended values [27].

			$Z = 7$				$Z = 8$			
$l_1l_2\ LSJ$	$l_3l_4\ L'S'J'$		λ	A	f	S	λ	A	f	S
$2s2p\,^3P_2$	$2p3p\,^3P_2$	a	233.966	3.76(09)	3.09(−2)	1.19(−1)	164.557	9.87(09)	4.01(−2)	1.09(−1)
		b		3.57(09)	2.93(−2)	1.13(−1)		9.77(09)	3.97(−2)	1.08(−1)
$2s2p\,^3P_1$	$2p3p\,^3P_1$	a	233.938	1.20(09)	9.82(−3)	2.27(−2)	164.526	3.07(09)	1.25(−2)	2.03(−2)
		b		1.19(09)	9.78(−3)	2.26(−2)		3.06(09)	1.24(−2)	2.02(−2)
$2s2p\,^3P_2$	$2p3p\,^3P_1$	a	234.017	2.19(09)	1.08(−2)	4.15(−2)	164.609	5.86(09)	1.43(−2)	3.87(−2)
		b		1.98(09)	9.78(−3)	3.77(−2)		5.76(09)	1.40(−2)	3.81(−2)
$2s2p\,^3P_1$	$2p3p\,^3P_0$	a	233.967	5.00(09)	1.37(−2)	3.16(−2)	164.557	1.31(10)	1.77(−2)	2.88(−2)
		b		4.76(09)	1.30(−2)	3.02(−2)		1.29(10)	1.75(−2)	2.85(−2)
$2s2p\,^3P_1$	$2p3p\,^3P_2$	a	233.887	1.23(09)	1.68(−2)	3.89(−2)	164.474	3.20(09)	2.16(−2)	3.51(−2)
		b		1.19(09)	1.63(−2)	3.77(−2)		3.14(09)	2.12(−2)	3.45(−2)
$2s2p\,^3P_0$	$2p3p\,^3P_1$	a	233.903	1.61(09)	3.96(−2)	3.05(−2)	164.489	4.15(09)	5.05(−2)	2.74(−2)
		b		1.59(09)	3.91(−2)	3.02(−2)		4.10(09)	4.99(−2)	2.71(−2)
$2s2p\,^3P_2$	$2p3p\,^3S_1$	a	236.741	3.37(09)	1.70(−2)	6.62(−2)	166.106	7.74(09)	1.92(−2)	5.26(−2)
		b		5.12(09)	2.49(−2)	9.50(−2)		7.97(09)	1.98(−2)	5.42(−2)
$2s2p\,^3P_1$	$2p3p\,^3S_1$	a	236.660	2.14(09)	1.79(−2)	4.19(−2)	166.021	5.09(09)	2.10(−2)	3.45(−2)
		b		3.08(09)	2.49(−2)	5.70(−2)		5.22(09)	2.16(−2)	3.54(−2)
$2s2p\,^3P_0$	$2p3p\,^3S_1$	a	236.624	7.31(08)	1.84(−2)	1.43(−2)	165.983	1.77(09)	2.19(−2)	1.20(−2)
		b		1.03(09)	2.49(−2)	1.90(−2)		1.82(09)	2.25(−2)	1.23(−2)
$2s2p\,^3P_2$	$2p3p\,^3D_3$	a	239.443	2.38(09)	2.87(−2)	1.13(−1)	167.915	6.52(09)	3.86(−2)	1.07(−1)
		b		3.19(09)	3.85(−2)	1.52(−1)		7.46(09)	4.42(−2)	1.22(−1)
$2s2p\,^3P_1$	$2p3p\,^3D_2$	a	239.447	1.80(09)	2.58(−2)	6.10(−2)	167.918	4.94(09)	3.48(−2)	5.78(−2)
		b		2.40(09)	3.44(−2)	8.14(−2)		5.66(09)	3.99(−2)	6.62(−2)
$2s2p\,^3P_0$	$2p3p\,^3D_1$	a	239.466	1.33(09)	3.44(−2)	2.71(−2)	167.935	3.66(09)	4.64(−2)	2.57(−2)
		b		1.77(09)	4.58(−2)	3.62(−2)		4.19(09)	5.31(−2)	2.94(−2)
$2s2p\,^3P_2$	$2p3p\,^3D_2$	a	239.530	5.83(08)	5.02(−3)	1.98(−2)	168.005	1.57(09)	6.66(−3)	1.84(−2)
		b		7.98(08)	6.87(−3)	2.71(−2)		1.79(09)	7.58(−3)	2.10(−2)
$2s2p\,^3P_1$	$2p3p\,^3D_1$	a	239.503	9.85(08)	8.48(−3)	2.00(−2)	167.974	2.67(09)	1.13(−2)	1.88(−2)
		b		1.33(09)	1.15(−2)	2.71(−2)		3.04(09)	1.29(−2)	2.14(−2)
$2s2p\,^3P_2$	$2p3p\,^3D_1$	a	239.586	6.39(07)	3.30(−4)	1.30(−3)	168.061	1.71(08)	4.35(−4)	1.21(−3)
		b		8.86(07)	4.58(−4)	1.81(−3)		1.95(08)	4.97(−4)	1.38(−3)
$2s2p\,^3P_2$	$2s3d\,^3D_3$	a	283.339	3.05(10)	5.15(−1)	2.40(0)	192.815	7.03(10)	5.49(−1)	1.74(0)
		b		3.05(10)	5.14(−1)	2.40(0)		6.89(10)	5.38(−1)	1.71(0)
$2s2p\,^3P_1$	$2s3d\,^3D_2$	a	283.228	2.29(10)	4.59(−1)	1.28(0)	192.708	5.28(10)	4.90(−1)	9.33(−1)
		b		2.29(10)	4.59(−1)	1.29(0)		5.17(10)	4.82(−1)	9.15(−1)
$2s2p\,^3P_0$	$2s3d\,^3D_1$	a	283.182	1.70(10)	6.13(−1)	5.71(−1)	192.661	3.91(10)	6.54(−1)	4.14(−1)
		b		1.69(10)	6.12(−1)	5.71(−1)		3.83(10)	6.41(−1)	4.07(−1)
$2s2p\,^3P_2$	$2s3d\,^3D_2$	a	283.344	7.63(09)	9.19(−2)	4.29(−1)	192.822	1.76(10)	9.81(−2)	3.11(−1)
		b		7.61(09)	9.18(−2)	4.28(−1)		1.72(10)	9.60(−2)	3.05(−1)
$2s2p\,^3P_1$	$2s3d\,^3D_1$	a	283.233	1.27(10)	1.53(−1)	4.28(−1)	192.713	2.93(10)	1.63(−1)	3.11(−1)
		b		1.27(10)	1.53(−1)	4.28(−1)		2.88(10)	1.60(−1)	3.05(−1)
$2s2p\,^3P_2$	$2s3d\,^3D_1$	a	283.349	8.48(08)	6.13(−3)	2.86(−2)	192.827	1.96(09)	6.54(−3)	2.08(−2)
		b		8.46(08)	6.12(−3)	2.86(−2)		1.91(09)	6.40(−3)	2.03(−2)
$2s2p\,^3P_2$	$2s3s\,^3S_1$	a	322.005	5.38(09)	5.02(−2)	2.66(−1)	214.998	1.09(10)	4.55(−2)	1.61(−1)
		b		4.99(09)	4.68(−2)	2.48(−1)		1.02(10)	4.23(−2)	1.50(−1)
$2s2p\,^3P_1$	$2s3s\,^3S_1$	a	321.854	3.23(09)	5.01(−2)	1.59(−1)	214.856	6.56(09)	4.54(−2)	9.63(−2)
		b		3.00(09)	4.68(−2)	1.49(−1)		6.09(09)	4.22(−2)	8.97(−2)
$2s2p\,^3P_0$	$2s3s\,^3S_1$	a	321.788	1.07(09)	5.01(−2)	5.31(−2)	214.793	2.18(09)	4.53(−2)	3.21(−2)
		b		1.00(09)	4.68(−2)	4.97(−2)		2.03(09)	4.23(−2)	2.99(−2)

Table 5. (Continued)

			$Z = 7$				$Z = 8$			
$l_1l_2\ LSJ$	$l_3l_4\ L'S'J'$		λ	A	f	S	λ	A	f	S
2s2p ^{1}P$_1$	2p3p ^{1}S$_0$	*a*	265.077	1.19(09)	4.19(−3)	1.10(−2)	181.258	5.61(09)	9.23(−3)	1.65(−2)
		b		2.54(09)	8.57(−3)	2.20(−2)		5.13(09)	8.52(−3)	1.53(−2)
2s2p ^{1}P$_1$	2p3p ^{1}D$_2$	*a*	270.213	9.79(09)	1.79(−1)	4.77(−1)	185.431	2.39(10)	2.05(−1)	3.76(−1)
		b		9.70(09)	1.78(−1)	4.76(−1)		2.13(10)	1.83(−1)	3.36(−1)
2s2p ^{1}P$_1$	2p3p ^{1}P$_1$	*a*	283.725	8.23(09)	9.94(−2)	2.78(−1)	193.850	1.02(10)	1.08(−1)	2.08(−1)
		b		7.22(09)	8.83(−2)	2.49(−1)		1.73(10)	9.81(−2)	1.89(−1)
2s2p ^{1}P$_1$	2s3d ^{1}D$_2$	*a*	333.228	1.84(10)	5.10(−1)	1.68(0)	219.712	4.34(10)	5.24(−1)	1.14(0)
		b		1.84(10)	5.18(−1)	1.71(0)		4.29(10)	5.21(−1)	1.13(0)
2s2p ^{1}P$_1$	2s3s ^{1}S$_0$	*a*	382.441	4.02(09)	2.94(−2)	1.11(−1)	246.889	7.64(09)	2.33(−2)	5.68(−2)
		b		2.55(09)	1.92(−2)	7.32(−2)		5.59(09)	1.72(−2)	4.23(−2)

3. Results and discussion

We calculate line strengths, oscillator strengths, and transition probabilities for $2l_12l_2[LSJ]$–$2l_33l_4[L'S'J']$ lines for all ions with $Z = 6$–100. The results were calculated in both length and velocity forms but, in view of the gauge independence discussed above, only length-form results are presented in the following tables and figures. The theoretical energies used to evaluate oscillator strengths and transition probabilities are calculated using the second-order MBPT formalism developed in [25, 28].

Transition rates A (s^{-1}) for $2l_12l_2[LSJ]$–$2l_33l_4[L'S'J']$ lines are given in figures 5–8. Each figure shows transitions to a fixed LSJ state from states belonging to a *complex* of states $2l_33l_4[LS]$. A complex includes all states of the same parity and J obtained from combinations of $2l_33l_4[LS]$ states. For example, the odd-parity complex with $J = 1$ includes states: 2s3p ^{1}P$_1$, 2s3p ^{3}P$_1$, 2p3s ^{3}P$_1$, 2p3s ^{1}P$_1$, 2p3d ^{3}D$_1$, 2p3d ^{3}P$_1$, 2p3d ^{1}P$_1$ in LS coupling, or 2s3p$_{1/2}$[1], 2s3p$_{3/2}$[1], 2p$_{1/2}$3s[1], 2p$_{3/2}$3s[1], 2p$_{1/2}$3d$_{3/2}$[1], 2p$_{3/2}$3d$_{3/2}$[1], 2p$_{3/2}$3d$_{5/2}$[1] in jj coupling. Later, we use the LS designations since they are more conventional. In figures 5 and 6, we present transition probabilities from levels of the odd-parity complex states with J=1 into the two even-parity $2l_12l_2$ states 2s^2 ^{1}S$_0$ and 2p^2 ^{1}D$_2$, respectively. Transition rates into the 2s2p ^{1}P$_1$ level from the even-parity complex with $J = 1$ are presented in figure 7 and those from the even-parity $J = 2$ complex are presented in figure 8.

The 2s2p ^{1}P$_1$–2s3s ^{1}S$_0$ transition shown in figure 5 was investigated by Smith *et al* [32] for ions with $Z = 4$–26 in 1973. In figure 6, there is a double cusp in the $Z = 35$–36 range which can be explained by crossing of the 2p3s ^{1}P$_1$ and 2p3d ^{3}D$_1$ levels. These two levels are very close in this interval, the energy splitting being less than 1% of the level separation within the complex. We observe in figure 6 that the curve describing the 2p^2 ^{1}D$_2$ − 2p3s ^{1}P$_1$ transition is smooth provided that the label 2p3s ^{1}P$_1$ is changed into the label 2p3d ^{3}D$_1$. Other singularities are also found for the A-values of the transitions 2p^2 ^{1}D$_2$–2p3s ^{3}P$_1$ in figure 6, 2s2p ^{1}P$_1$–2p3p ^{3}P$_1$ in figure 7, and 2s2p ^{1}P$_1$–2s3d ^{3}D$_2$ in figure 8. All of these are LS-forbidden transitions. It is worth noting that the singularities occur when the A-values for a given transition become very small compared with the other A-values within a given complex.

We note that the A-values for LS-forbidden transitions can become dominant for high Z as seen, e.g., in the transitions 2s^2 ^{1}S$_0$–2p3s ^{3}P$_1$ in figure 5, 2p^2 ^{1}D$_2$–2p3d ^{3}P$_1$ in figure 6, and 2s2p ^{1}P$_1$–2p3p ^{3}P$_1$ in figure 7. This occurs because LS coupling gradually changes to jj coupling as Z increases. For example, the LS-forbidden transition 2s2p ^{1}P$_1$–2p3p ^{3}P$_1$ becomes the jj-allowed transition 2s2p$_{3/2}$[1]–2p$_{3/2}$3p$_{3/2}$[1] at high Z. We also note that the

Table 6. Wavelengths λ (Å), oscillator strengths f, and transition rates A (s^{-1}) for the $2s^2\,{}^1S_0$–$2s3p\,{}^1P_1$ transition. Present calculations[a] compared with other theoretical values[b–e] and experimental values[g].

Z	λ^a	f^a	$f^{b,e}$	A^a	$A^{c,d}$	A^g
6	85.64	0.267	0.241[b]	3.99(09)	3.45(09)[d]	2.95(09)
7	47.13	0.341	0.334[b]	1.24(10)	1.13(10)[c]	1.04(10)
8	72.16	0.399	0.400[b]	2.99(10)	2.84(10)[c]	2.65(10)
9	26.93	0.445	0.450[b]	6.14(10)	5.98(10)[c]	5.62(10)
10	7.503	0.480	0.488[b]	1.12(11)	1.10(11)[c]	1.05(11)
11	7.269	0.508		1.89(11)	1.87(11)[c]	1.80(11)
12	2.750	0.528	0.538[e]	2.98(11)	2.96(11)[c]	2.86(11)
13	1.975	0.539	0.550[e]	4.43(11)	4.42(11)[c]	4.29(11)
14	3.756	0.540	0.553[e]	6.27(11)	6.27(11)[c]	6.09(11)
15	7.342	0.529	0.543[e]	8.43(11)	8.43(11)[c]	8.22(11)
16	2.242	0.503	0.521[e]	1.08(12)	1.08(12)[c]	1.06(12)
17	8.118	0.467	0.489[e]	1.31(12)		1.33(12)
18	4.736	0.425	0.455[e]	1.54(12)	1.59(12)[c]	1.58(12)
19	1.928	0.386	0.429[e]	1.78(12)		1.83(12)
20	9.572	0.352	0.416[e]	2.04(12)	2.11(12)[c]	2.08(12)
21	7.574	0.324	0.390[e]	2.33(12)		2.37(12)
22	5.866	0.303	0.325[e]	2.67(12)		2.75(12)
23	4.394	0.286	0.301[e]	3.07(12)		3.15(12)
24	3.116	0.274	0.286[e]	3.54(12)		3.83(12)
25	2.000	0.265	0.274[e]	4.08(12)		4.43(12)
26	1.020	0.258	0.265[e]	4.71(12)	4.86(12)[c]	5.13(12)
27	0.154	0.252	0.259[e]	5.44(12)		
28	9.385	0.249	0.258[e]	6.27(12)		
29	8.699	0.246	0.249[e]	7.22(12)		
30	8.085	0.244	0.249[e]	8.30(12)		
32	7.035	0.242	0.246[e]	1.09(13)		
34	6.173	0.242	0.245[e]	1.41(13)		
36	5.459	0.243	0.245[e]	1.81(13)	1.84(13)[c]	
38	4.859	0.244	0.234[e]	2.30(13)		
40	4.351	0.246	0.236[e]	2.89(13)		
42	3.916	0.248	0.238[e]	3.59(13)		
44	3.542	0.250	0.240[e]	4.42(13)		
45	3.374	0.251	0.241[e]	4.89(13)		
46	3.218	0.251	0.243[e]	5.40(13)		
47	3.071	0.252	0.244[e]	5.94(13)		
48	2.934	0.253	0.245[e]	6.53(13)		
49	2.806	0.254	0.246[e]	7.17(13)		
50	2.685	0.255	0.247[e]	7.85(13)		
52	2.465	0.256	0.248[e]	9.36(13)		
54	2.270	0.257	0.250[e]	1.11(14)		

[a] Present calculations.
[b] Froese Fischer *et al* [16].
[c] Fritzsche and Grant [22].
[d] Eissner and Tully [8].
[e] Kim *et al* [21].
[g] Curtis *et al* [36].

Z-dependence of uncoupled matrix elements are smooth functions of Z and singularities occur only after coupling.

Table 7. Wavelengths λ (Å), oscillator strengths f, transition rates A (s^{-1}) for the $2s^2\ ^1S_0$–$2s3p\ ^3P_1$ transition. Present calculations[a] compared with other theoretical values[b–e] and experimental values[g].

Z	λ^a	f^a	f^b	A^a	A^c	A^d	A^e	A^g
6	384.55	0.000 01		8.41(04)			5.0(05)	4(05)
7	246.17	0.000 04		1.33(06)	1.40(06)	4.97(06)	3.2(06)	2.8(06)
8	171.51	0.000 16		1.17(07)	1.64(07)	2.22(07)	1.96(07)	1.9(07)
9	126.50	0.000 52		7.15(07)	8.55(07)	9.59(07)	9.89(07)	1.00(08)
10	97.213	0.001 4		3.38(08)	3.85(08)	3.70(08)	4.15(08)	4.18(08)
11	77.067	0.003 6		1.33(09)	1.55(09)	1.27(09)		1.68(09)
12	62.606	0.008 1	0.022	4.56(09)	4.72(09)	3.97(09)		5.76(09)
13	51.869	0.017	0.032	1.39(10)	1.39(10)	1.13(10)		1.76(10)
14	43.676	0.033	0.047	3.83(10)	3.70(10)	2.97(10)		4.77(10)
15	37.280	0.059	0.069	9.47(10)	9.33(10)	7.21(10)		1.11(11)
16	32.190	0.097	0.102	2.09(11)	2.02(11)	1.60(11)		2.23(11)
17	28.074	0.145	0.145	4.10(11)				4.10(11)
18	24.696	0.196	0.195	7.16(11)	6.67(11)	5.93(11)		7.11(11)
19	21.891	0.245	0.245	1.13(12)				1.15(12)
20	19.535	0.287	0.334	1.67(12)	1.60(12)	1.52(12)		1.73(12)
21	17.537	0.321	0.343	2.32(12)				2.43(12)
22	15.829	0.348	0.355	3.09(12)		3.00(12)		3.22(12)
23	14.357	0.370	0.371	3.99(12)				4.22(12)
24	13.079	0.387	0.387	5.03(12)		4.06(12)		5.13(12)
25	11.962	0.401	0.400	6.22(12)				6.39(12)
26	10.981	0.411	0.411	7.58(12)	4.86(12)	5.30(12)		7.85(12)
27	10.115	0.420	0.420	9.12(12)				
28	9.346	0.426	0.426	1.08(13)				
29	8.660	0.431	0.431	1.28(13)				
30	8.045	0.434	0.435	1.49(13)				
32	6.994	0.437	0.439	1.99(13)				
34	6.133	0.437	0.438	2.60(13)				
36	5.418	0.432	0.434	3.27(13)	3.24(13)			
38	4.818	0.425	0.419	4.07(13)				
40	4.310	0.413	0.407	4.94(13)				
42	3.876	0.396	0.386	5.86(13)				
44	3.502	0.372	0.356	6.74(13)				
45	3.335	0.356	0.336	7.11(13)				
46	3.179	0.337	0.311	7.40(13)				
47	3.033	0.313	0.276	7.57(13)				
48	2.896	0.286	0.190	7.58(13)				
49	2.769	0.255	0.181	7.39(13)				
50	2.649	0.221	0.167	6.99(13)				
52	2.431	0.151	0.115	5.68(13)				
54	2.238	0.094	0.071	4.19(13)				

[a] Present calculations.
[b] Kim *et al* [21].
[c] Fritzsche and Grant [22].
[d] Eissner and Tully [8].
[e] Froese Fischer *et al* [17].
[g] Curtis *et al* [36].

In table 4, we give transition probabilities A, oscillator strengths f, and line strengths S for allowed even–odd transitions $2s^2$–2s3p, $2p^2$–2p3s, and $2p^2$–2p3d for the two low-Z ions N^{3+} and O^{4+}. Results from the present calculations are listed in rows labelled *a* and values

recommended by NIST given in [27] are listed in rows labelled b. In table 5, we give a similar tabulation of A, f, and S for allowed odd–even transitions 2s2p–2s3s and 2s2p–2s3d in N^{3+} and O^{4+}. We find reasonably good agreement (5–50%) between our data and the NIST data for N^{3+} and see that the agreement improves for O^{4+}, in accordance with the expected accuracy of MBPT calculations. It should be emphasized that the accuracy of our data improves with increasing Z, owing to the better convergence of MBPT for higher values of nuclear charge.

In tables 6 and 7, we compare our f- and A-values for two transitions $2s^2\,{}^1S_0$–$2s3p\,{}^1P_1$ and $2s^2\,{}^1S_0$–$2s3p\,{}^3P_1$ with theoretical [4, 8, 16, 17, 21, 22] and experimental [33–36] data in the range $Z = 6$–54. There are other decay channels from the levels $2s3p\,{}^1P_1$ and $2s3p\,{}^3P_1$ besides the one to the ground state; namely, decays to the $2s3s\,{}^1S_0$ and $2s3s\,{}^3S_1$ states. The A-values for the $2s3s\,{}^3S_1$–$2s3p\,{}^3P_1$ transitions are much larger than those for the $2s^2\,{}^1S_0$–$2s3p\,{}^3P_1$ transitions for $Z = 6$, 7, and 8 as seen in table 7. The agreement between various A- and f-values for allowed transitions presented in table 6 is very good. By contrast, the A-values for intercombination transitions are very sensitive to different theoretical methods and the agreement is poor, as seen in table 7.

4. Conclusion

We have presented a systematic second-order relativistic MBPT study of reduced matrix elements, oscillator strengths, and transition rates for allowed and forbidden $2l$–$3l'$ electric-dipole transitions in Be-like ions with nuclear charges ranging from $Z = 6$ to 100. The retarded dipole matrix elements include correlation corrections from Coulomb and Breit interactions. Contributions from NESs were also included in the second-order matrix elements. Both length and velocity forms of the matrix elements were evaluated, and small differences, caused by the non-locality of the starting HF potential, were found between the two forms. Second-order MBPT transition energies were used to evaluate oscillator strengths and transition rates. Our theoretical data for allowed transitions agree with experiment within the experimental uncertainties for the $2s2p\,{}^1P_1$ level. We believe that these results will be useful in analysing existing experimental data and planning new experiments. Additionally, the matrix elements from the present calculations provide basic theoretical input for calculations of reduced matrix elements, oscillator strengths, and transition rates in three-electron boron-like ions.

Acknowledgments

The work of WRJ, MSS and AD was supported in part by National Science Foundation Grant No PHY-95-13179. UIS acknowledges partial support by grant no B336454 from Lawrence Livermore National Laboratory.

Appendix. MBPT formulae

The first-order reduced K-pole matrix element $Z_K^{(1)}$ for transitions between two states $vw(J)$ and $v'w'(J')$ is [24]

$$Z_K^{(1)}[v_1w_1(J)\text{–}v_2w_2(J')] = \sqrt{[J][J']}\sum_{vw}\sum_{v'w'}\mathcal{S}^J(v_1w_1, vw)\mathcal{S}^{J'}(v_2w_2, v'w') \times(-1)^{K+j_w+j_{v'}}\left\{\begin{array}{ccc} J & J' & K \\ j_{v'} & j_w & j_v \end{array}\right\} Z_K(v'w)\delta_{vw'}, \tag{A1}$$

where $[J] = 2J + 1$. The quantity $\mathcal{S}^J(v_1w_1, vw)$ is a symmetry coefficient defined by

$$\mathcal{S}^J(v_1w_1, vw) = \eta_{v_1w_1}[\delta_{v_1v}\delta_{w_1w} + (-1)^{j_v+j_w+J+1}\delta_{v_1w}\delta_{w_1v}], \tag{A2}$$

where η_{vw} is a normalization factor given by

$$\eta_{vw} = \begin{cases} 1 & \text{for} \quad w \neq v \\ 1/\sqrt{2} & \text{for} \quad w = v. \end{cases}$$

The dipole matrix element $Z_1(vw) = \frac{3}{k}\langle v\|t_1^{(1)}\|w\rangle$, which includes retardation, is given in length and velocity forms by equations (38), (39) of [24] and equations (3), (4) of [1].

The second-order reduced matrix element $Z_K^{(2)}$ for the transition between the two states $vw(J)$–$v'w'(J')$ consists of four contributions: $Z_K^{(\mathrm{HF})}$, $Z_K^{(\mathrm{RPA})}$, $Z_K^{(\mathrm{corr})}$, and $Z_K^{(\mathrm{derv})}$:

$$Z_K^{(\mathrm{HF})}[v_1w_1(J)\text{–}v_2w_2(J')] = \sqrt{[J][J']}\sum_{vw}\sum_{v'w'}\mathcal{S}^J(v_1w_1, vw)\mathcal{S}^{J'}(v_2w_2, v'w')$$
$$\times(-1)^{K+j_w+j_{v'}}\begin{Bmatrix} J & J' & K \\ j_{v'} & j_w & j_v \end{Bmatrix}\sum_i\left[\frac{Z_K(v'i)\Delta_{iw}}{\varepsilon_i-\varepsilon_w}+\frac{Z_K(iw)\Delta_{v'i}}{\varepsilon_i-\varepsilon_{v'}}\right]\delta_{vw'}, \quad \text{(A3)}$$

$$Z_K^{(\mathrm{RPA})}[v_1w_1(J)\text{–}v_2w_2(J')] = \frac{1}{2K+1}\sqrt{[J][J']}\sum_{vw}\sum_{v'w'}\mathcal{S}^J(v_1w_1, vw)\mathcal{S}^{J'}(v_2w_2, v'w')$$
$$\times(-1)^{j_{w'}+j_v}\begin{Bmatrix} J & J' & K \\ j_{v'} & j_w & j_v \end{Bmatrix}$$
$$\times\sum_n\sum_b\left[\frac{Z_K(bn)Z_K(wbv'n)}{\varepsilon_n+\varepsilon_{v'}-\varepsilon_w-\varepsilon_b}+\frac{Z_K(nb)Z_K(wnv'b)}{\varepsilon_n+\varepsilon_w-\varepsilon_{v'}-\varepsilon_b}\right]\delta_{vw'}, \quad \text{(A4)}$$

$$Z_K^{(\mathrm{corr})}[v_1w_1(J)\text{–}v_2w_2(J')]$$
$$= \sqrt{[J][J']}\sum_{vw}\sum_{v'w'}\mathcal{S}^J(v_1w_1, vw)\mathcal{S}^{J'}(v_2w_2, v'w')\sum_k(-1)^{K+k}\sum_i$$
$$\times\left[\frac{Z_K(iv)X_k(v'w'wi)}{\varepsilon_i+\varepsilon_w-\varepsilon_{v'}-\varepsilon_{w'}}\begin{Bmatrix} J & J' & K \\ j_i & j_v & j_w \end{Bmatrix}\begin{Bmatrix} j_i & j_w & J' \\ j_{v'} & j_{w'} & k \end{Bmatrix}(-1)^{J+j_w+j_{w'}}\right.$$
$$\left.+\frac{Z_K(v'i)X_k(iw'vw)}{\varepsilon_i+\varepsilon_{w'}-\varepsilon_v-\varepsilon_w}\begin{Bmatrix} J' & J & K \\ j_i & j_{v'} & j_{w'} \end{Bmatrix}\begin{Bmatrix} j_i & j_{w'} & J \\ j_w & j_v & k \end{Bmatrix}(-1)^{j_v+j_{v'}}\right]. \quad \text{(A5)}$$

In the above equations, the index b designates core states, n designates virtual (excited) states, and i denotes an arbitrary core or excited state. In the sums over i in equation (A3), all terms with vanishing denominators are excluded. In the sum occurring in the first term of equation (A5), states i for which (iw) is in the model space of final states $(v'w')$ are excluded, while in the second term, states i for which (iw') is in the model space of initial states (vw) are excluded. In the sums over n in the RPA matrix elements (A4), all core states are excluded.

We denote the two-particle Coulomb + Breit interaction integral including direct and exchange parts by $Z_k(abcd)$. The Coulomb contributions are given by

$$Z_k(bcmn) = X_k(bcmn) + \sum_{k'}[k]\begin{Bmatrix} j_b & j_m & k \\ j_c & j_n & k' \end{Bmatrix}X_{k'}(bcnm), \quad \text{(A6)}$$

where

$$X_k(abcd) = \langle a|\,|C_k|\,|c\rangle\langle b||C_k||d\rangle R_k(abcd). \quad \text{(A7)}$$

In the above equation, C_k are normalized spherical harmonics and $R_k(abcd)$ are Slater integrals. To include the Breit interaction, the Coulomb matrix element $X_k(abcd)$ must be modified according to the rule:

$$X_k(abcd) \to X_k(abcd) + M_k(abcd) + N_k(abcd). \quad \text{(A8)}$$

The magnetic radial integrals M_k and N_k are defined by equations (A4), (A5) in [37]. The quantity Δ_{ij} in equation (A3) is defined as:

$$\Delta_{ij} = \sum_a \delta_{j_i j_j} \sqrt{\frac{[j_a]}{[j_i]}} Z_0(iaja), \tag{A9}$$

for the Coulomb case (for details see [28].

The second-order reduced matrix element of the derivative term is given by:

$$Z_K^{(\mathrm{derv})}[vw(J)\text{–}v'w'(J')] = \alpha(E_{vw}^{(1)} - E_{v'w'}^{(1)}) P_K^{(\mathrm{derv})}[vw(J)\text{–}v'w'(J')], \tag{A10}$$

where $E_{vw}^{(1)}$ is the first-order correction to the energy defined by equations (2.8)–(2.10) in [28], and α is the fine-structure constant. The quantity $P^{(\mathrm{derv})}$ is given by

$$P_K^{(\mathrm{derv})}[v_1w_1(J)\text{–}v_2w_2(J')] = \sqrt{[J][J']} \sum_{vw} \sum_{v'w'} \mathcal{S}^J(v_1w_1, vw)\mathcal{S}^{J'}(v_2w_2, v'w') \tag{A11}$$

$$\times(-1)^{K+j_w+j_{v'}} \left\{ \begin{array}{ccc} J & J' & K \\ j_{v'} & j_w & j_v \end{array} \right\} Z_K^{(\mathrm{derv})}(v'w)\delta_{vw'}. \tag{A12}$$

The expression for $Z_K^{(\mathrm{derv})}(vw)$ is obtained from $\langle v \| \frac{\mathrm{d}_K^{(1)}}{\mathrm{d}k} \| w \rangle$ and given by equations (10) and (11) in [1] for $K = 1$.

References

[1] Safronova U I, Johnson W R, Safronova M S and Derevianko A 1999 *Phys. Scr.* **59** 286
[2] Boiko V A, Pikuz S A, Safronova U I and Faenov A Ya 1977 *J. Phys. B: At. Mol. Phys.* **10** 1253
[3] Safronova U I 1986 *Opt. Spectrosc.* **60** 10
[4] Ralchenko Y V and Vainshtein L A 1995 *Phys. Rev.* A **52** 2449
[5] Nusbaumer H 1972 *Astron. Astrophys.* **16** 77
[6] Victor G A and Laughlin C 1973 *Nucl. Instrum. Methods* **110** 189
[7] Bhatia A K, Feldman U and Seely J F 1986 *At. Data Nucl. Data Tables* **35** 449
[8] Eissner W B and Tully J A 1992 *Astron. Astrophys.* **253** 625
[9] Hibbert A 1979 *J. Phys. B: At. Mol. Phys.* **12** L661
[10] Hibbert A 1980 *J. Phys. B: At. Mol. Phys.* **13** 17211
[11] Sampson D H, Clark R E H and Goett S J 1981 *Phys. Rev.* A **24** 2979
[12] Chang T N and Chang X 1990 *J. Quant. Spectrosc. Radiat. Transfer* **43** 207
[13] Chang T N and Mu Y 1990 *J. Quant. Spectrosc. Radiat. Transfer* **44** 413
[14] Ellis D G 1983 *Phys. Rev.* A **28** 1223
[15] Fawcett B C 1984 *At. Data Nucl. Data Tables* **30** 1
[16] Froese Fischer C, Godefroid M and Olsen J 1997 *J. Phys. B: At. Mol. Opt. Phys.* **30** 1163
[17] Froese Fischer C, Gaigalas G and Godefroid M 1997 *J. Phys. B: At. Mol. Opt. Phys.* **30** 3333
[18] Tully J A, Seaton M J and Berrington K A 1990 *J. Phys. B: At. Mol. Opt. Phys.* **23** 3811
[19] Ramsbotton C A, Berrington K A, Hibbert A and Bell K L 1994 *Phys. Scr.* **50** 246
[20] Verner D A, Verner E M and Ferland G J 1996 *At. Data Nucl. Data Tables* **64** 1
[21] Kim Y Ki, Martin W C and Weiss A W 1988 *J. Opt. Soc. Am.* B **5** 2215
[22] Fritzsche S and Grant I P 1994 *Phys. Scr.* **50** 473
[23] Charro E, Martin I and Lavin C 1996 *J. Quant. Spectrosc. Radiat. Transfer* **34** 241
[24] Johnson W R, Plante D R and Sapirstein J 1995 *Adv. At. Mol. Phys.* **35** 255
[25] Safronova M S, Johnson W R and Safronova U I 1997 *J. Phys. B: At. Mol. Opt. Phys.* **30** 2375
[26] Sucher J 1980 *Phys. Rev.* A **22** 348
Mittleman M H 1981 *Phys. Rev.* A **24** 1167
[27] Wiese W L, Fuhr J R and Deters T M 1996 *J. Phys. Chem. Ref. Data* **7**
[28] Safronova M S, Johnson W R and Safronova U I 1996 *Phys. Rev.* A **53** 4036
[29] Johnson W R, Liu Z W and Sapirstein J 1996 *At. Data Nucl. Data Tables* **64** 279
[30] Lindgren I and Morrison J 1985 *Atomic Many-Body Theory* 2nd edn (Berlin: Springer)
[31] Derevianko A, Savukov I, Johnson W R and Plante D R 1998 *Phys. Rev.* A **58** 1016
[32] Smith M W, Martin G A and Wiese W L 1973 *Nucl. Instrum. Methods* **110** 219

[33] Engström L, Denne B, Huldt S, Ekberg J O, Curtis L J, Veje E and Martinson I 1979 *Phys. Scr.* **20** 88
[34] Hardis J E, Curtis L J, Ramanujam P S, Livingston A E and Brooks R L 1983 *Phys. Rev.* A **27** 257
[35] Granzov J, Heckmann P H and Träbert E 1994 *Phys. Scr.* **49** 148
[36] Curtis L J *et al* 1995 *Phys. Rev.* A **51** 4575
[37] Chen M H, Cheng K T and Johnson W R 1993 *Phys. Rev.* A **47** 3692